Agrotechniques in Industrial Crops

Journal Homepage: https://atic.razi.ac.ir

Silver Nanoparticle–Elicited Reprogramming of Metabolism and Anticancer Activity in *Calotropis procera* Callus Cultures

Soheila Noori[*1,2], **Hamideh Khaje**[2]

[1]*Department of Range and Watershed Management, Faculty of Water and Soil, University of Zabol, Zabol, Iran*
[2]*Agricultural Biotechnology Research Institute, University of Zabol, Zabol, Iran*

ARTICLE INFO

Original paper

Article history:
Received: xx xxx 202x
Revised: xx xxx 202x
Accepted: xx xxx 202x

Keywords:
Anticancer activity
Antioxidant defense
Bioactive potential
Biological efficacy
Calotropis procera
Metabolic elicitation
Molecular level

ABSTRACT

Calotropis procera is a multipurpose medicinal plant with recognized bioactive potential. this is a, which can be utilized for medicine, fodder, fuel purposes, timber, fibre production, phytoremediation; however, its controlled production of pharmacologically relevant metabolites remains challenging. In the present study, an in vitro callus culture system of *C. procera* was established and subjected to silver nanoparticle (AgNP) elicitation to enhance metabolic activity and biological efficacy. AgNP treatment significantly improved callus growth and biomass accumulation, accompanied by marked alterations in primary metabolism, including increased carbohydrate and protein contents. Secondary metabolite production was strongly stimulated, as evidenced by elevated phenolic and flavonoid levels and enhanced antioxidant capacity. AgNP elicitation also induced differential regulation of antioxidant defense enzymes, indicating a coordinated metabolic and redox reprogramming rather than a generalized stress response. Bioactive extracts obtained from AgNP-treated callus exhibited a pronounced, dose-dependent cytotoxic effect against MCF-7 human breast cancer cells, with a significantly reduced IC_{50} value compared with non-elicited callus extracts. At the molecular level, treatment with AgNP-elicited callus extracts promoted a pro-apoptotic gene expression profile, characterized by upregulation of BAX and concurrent downregulation of BCL2, NFKB1, and TLR4, suggesting suggesting activation of pro-apoptotic signaling pathwaysand suppression of pro-survival and inflammatory signaling pathways. Collectively, these findings demonstrate that AgNP-assisted elicitation effectively reprograms metabolic and molecular pathways in *C. procera* callus cultures, generating bioactive extracts with enhanced anticancer properties. This strategy offers a promising, sustainable platform for the production of plant-derived anticancer agents.

DOI: 10.22126/ATIC.2026.13560.1270
© The Author(s) 202x. Published by Razi University

1. Introduction

The search for novel therapeutic agents from natural sources remains a cornerstone of modern pharmaceutical research, particularly in oncology, where resistance to conventional chemotherapies continues to challenge clinical outcomes (Newman and Cragg, 2020). In Iran, this plant is found in the tropical regions and the southern coast of the Sea of Oman from Khuzestan to Makran in Balochistan at an altitude of 1100 meters above sea level. Phytochemical investigations have revealed that C. procera is a rich reservoir of bioactive secondary metabolites, including cardenolides, flavonoids, and phenolic compounds with known bioactive properties (Murti *et al*., 2010; Quazi *et al*., 2013). However, the commercial exploitation of these metabolites is frequently hindered by the limitations associated with harvesting field-grown plants, due to limitations associated with field-grown plants (Ochoa-Villarreal *et al*., 2016). To overcome these agronomic constraints, plant tissue culture (PTC) has emerged as a sustainable and controlled biotechnological platform for the continuous production of high-value plant metabolites (Ochoa-Villarreal *et al*., 2016). In particular, callus cultures provide a controlled system for metabolite production (Espinosa-Leal *et al*., 2018). Despite these advantages,

* Corresponding author.
E-mail address: snoori.327@uoz.ac.ir

undifferentiated callus cultures often yield lower concentrations of secondary metabolites compared to the intact mother plant due to the lack of organ-specific differentiation and environmental stress cues that typically trigger biosynthetic pathways (Murthy *et al*., 2014). Consequently, biotechnological strategies such as precursor feeding, metabolic engineering, and elicitation are frequently employed to enhance metabolic productivity in vitro (Narayani and Srivastava, 2017).

Elicitation, the application of biotic or abiotic stressors to plant cell cultures, is one of the most effective strategies to stimulate the synthesis of defense-related secondary metabolites (Ramirez-Estrada *et al*., 2016). Among abiotic elicitors, engineered nanomaterials have recently gained attention as potent modulators of plant physiology. Silver nanoparticles (AgNPs), in particular, act as novel elicitors. This "nanostress" activates the plant's antioxidant defense machinery and upregulates the expression of genes encoding key biosynthetic enzymes, leading to the accumulation of phenols, flavonoids, and other stress-responsive metabolites (Fazal *et al*., 2016). Studies on species such as *Artemisia annua* and *Linum usitatissimum* have demonstrated that AgNP elicitation can significantly reprogram cellular metabolism, resulting in superior bioactive profiles compared to non-elicited controls (Zhang *et al*., 2013).

The relevance of enhancing these phytochemical profiles is particularly pronounced in the context of cancer research. Breast cancer remains the most prevalent malignancy among women globally, necessitating the development of new therapeutic agents that can effectively target cancer cells while minimizing systemic toxicity (Bray *et al*., 2024). Plant-derived compounds often exert their anticancer effects by modulating complex molecular signaling pathways governing cell survival and death (Pfeffer and Singh, 2018). A critical mechanism of action for many chemotherapeutic agents is the suggestion of apoptosis-related molecular changes, the intrinsic programmed cell death pathway, which is regulated by the balance between pro-apoptotic proteins (e.g., BAX) and anti-apoptotic proteins (e.g., BCL-2) (Goldar *et al*., 2015).

Furthermore, recent evidence suggests that the therapeutic efficacy of natural products is also linked to the suppression of inflammatory pathways that fuel tumor progression (Saleh *et al*., 2021). The Nuclear Factor-kappa B (NF-κB) signaling pathway and its upstream activators, such as Toll-like Receptor 4 (TLR4), play pivotal roles in linking inflammation to cancer cell survival, proliferation, and resistance to apoptosis (Bateman *et al*., 2006; Perkins, 2012; Sato *et al*., 2009). While crude extracts of *C. procera* have shown cytotoxic potential, the specific molecular mechanisms by which AgNP-elicited callus extracts modulate the BAX/BCL-2 axis and the NF-κB/TLR4 signaling cross-talk in breast cancer cells remain largely unexplored.

The present study addresses this knowledge gap by integrating nanobiotechnology with plant tissue culture to establish a high-yielding production platform for bioactive metabolites. We hypothesized that controlled elicitation with AgNPs would induce a metabolic reprogramming in *C. procera* callus cultures, enhancing their antioxidant capacity and secondary metabolite content. Therefore, the objectives of this study were to: (1) evaluate the impact of AgNPs on the growth kinetics and oxidative stress response of *C. procera* callus; (2) profile the changes in primary and secondary metabolism induced by the nano-elicitor; and (3) determine the *in vitro* anticancer efficacy of the elicited extracts against MCF-7 human breast cancer cells, with a specific focus on the transcriptional modulation of apoptotic (*BAX*, *BCL2*) and inflammatory (*NFKB1*, *TLR4*) gene expression.

2. Materials and methods

2.1. Plant material and explant preparation

Fresh *C. procera* (Aiton) W.T.Aiton plant material was collected from the wild in Sistan and Baluchistan province, Iran (Noori *et al*., 2018). A voucher specimen was deposited at the Herbarium of Zabol University, Iran, under accession number ZU-CAL-2025 for future reference. To initiate aseptic cultures, mature seeds of *C. procera* were used as explants. The sterilized seeds were inoculated on hormone-free Murashige and Skoog (MS) basal medium and incubated at 25 ± 2°C with a 16 h light/8 h dark photoperiod (cool white fluorescent light, ~40 µmol $m^{-2}s^{-1}$). Seeds germinated within 1–2 weeks, yielding aseptic seedlings. Explants (~5 mm segments) were then prepared from young seedling tissues (cotyledon and hypocotyl) under sterile

conditions in a laminar flow hood. These explants served as the starting material for callus induction.

2.2. Callus induction and maintenance

Callus cultures were initiated on MS basal medium (full-strength macro- and micronutrients and vitamins). Sterilized explants (cotyledon and hypocotyl segments) were plated on the prepared medium in Petri dishes and incubated in a growth chamber at 25 ± 2°C in darkness for the first 7 days to encourage callus initiation. Thereafter, cultures were maintained under a 16 h light/8 h dark photoperiod (cool white fluorescent ~50 µmol $m^{-2}s^{-1}$) at 25°C. Under these conditions, friable callus formation was observed within 2–3 weeks. Induced calli were subcultured onto fresh MS medium of the same composition every 3–4 weeks to maintain vigorous growth. All cultures were handled aseptically, and at least three replicate explants were cultured per treatment to ensure reproducibility.

2.3. Synthesis of silver nanoparticles (AgNPs)

Silver nanoparticles were biosynthesized via a green synthesis approach using a plant extract as the reducing and capping agent. Fresh, healthy leaves of *C. procera* were collected, rinsed with tap water, and then washed with distilled water followed by 70% ethanol to remove surface contaminants. The leaves were air-dried and cut into small pieces. The decoction was cooled to room temperature, filtered through Whatman No. 1 filter paper, and the resulting *C. procera* leaf aqueous extract was stored at 4°C until use. For nanoparticle synthesis, an aqueous solution of silver nitrate ($AgNO_3$) (Sigma–Aldrich, St. Louis, MO, USA) was prepared at 4 mM. The leaf extract was added to the $AgNO_3$ solution at a 1:3 (v/v) extract-to-$AgNO_3$ ratio (e.g., 100 mL extract with 300 mL $AgNO_3$) under continuous stirring. The reaction mixture was incubated at 40°C for 4 h in the dark (to prevent photo-degradation), allowing the bio-reduction of Ag^+ to Ag^0. A visible color change of the solution from pale yellow to dark brown indicated the formation of silver nanoparticles. After synthesis, AgNPs were collected. The pellet containing AgNPs was washed twice by redispersing in deionized water and centrifuging again to remove any unreacted ions or residual plant metabolites. The purified AgNP pellet was then dried under vacuum at 60°C and stored as a powder at room temperature in the dark until characterization and use.

2.4. Characterization of AgNPs

The biosynthesized AgNPs were characterized by spectroscopic and microscopic techniques to confirm their formation, size, and morphology. A UV–Vis absorption spectrum of the nanoparticle colloid was recorded using a UV–Vis spectrophotometer (Cary 60, Agilent Technologies, Santa Clara, CA, USA) in the range of 300–600 nm. The appearance of a surface plasmon resonance peak between ~400–450 nm was taken as indicative of AgNP formation. The hydrodynamic diameter and polydispersity of the AgNPs were determined by dynamic light scattering (DLS) using a Malvern Zetasizer Nano ZS (Malvern Instruments, UK) at 25°C. The zeta potential was also measured by the same instrument to assess particle surface charge and colloidal stability. For microscopy, the size and morphology of AgNPs were examined by field-emission scanning electron microscopy (FE-SEM). Dried nanoparticle powder was mounted on a metal stub using carbon tape and sputter-coated with a thin layer of gold (≈10 nm) to improve conductivity. The sample was imaged using an FE-SEM (Nova NanoSEM 450, FEI, USA) operated at an accelerating voltage of 10 kV and high vacuum. Digital micrographs were analyzed to estimate the particle size range and shape. The AgNPs were expected to appear as roughly spherical particles in aggregated clusters, as commonly observed for plant-mediated AgNPs. All characterization instruments were properly calibrated, and measurements were performed in triplicate to ensure reliability.

2.5. AgNP elicitation of callus cultures

To investigate the elicitor effect of AgNPs on *C. procera* callus, established calli (~6 weeks old) were transferred to fresh solid MS medium (with the same 2,4-D and kinetin concentrations as used for maintenance) supplemented with sterile AgNPs. Uniform callus pieces of approximately 0.25 g fresh weight were inoculated onto AgNP-containing media to ensure equal biomass per treatment. AgNPs (from the stock powder) were first suspended in sterile distilled water and ultrasonicated for 10 min to prevent aggregation. The nanoparticle suspension was then added to molten autoclaved MS agar medium (cooled to ~45°C) to achieve final AgNP concentrations of 0, 125, 250, 500 ppm, based on previous studies showing effective elicitation ranges. The medium was poured

into Petri dishes under aseptic conditions and allowed to solidify. Control callus cultures received no AgNPs (0 ppm) but were otherwise treated identically. Callus cultures were incubated in a controlled growth chamber at 25°C under a 16 h light/8 h dark photoperiod (fluorescent light ~50 µmol $m^{-2}s^{-1}$) throughout the elicitation period. The elicitor exposure was maintained for 21 days, during which callus growth and morphology were monitored. At the end of the treatment, calli were harvested for analyses. Harvesting was done under sterile conditions; callus tissues were gently blotted to remove any medium, quickly rinsed with sterile distilled water to remove surface AgNPs, and frozen in liquid nitrogen to quench metabolism. The samples were stored at –80°C or lyophilized (for certain assays) until further use. All treatments were set up in triplicate (three independent Petri dishes per AgNP concentration), and the entire elicitation experiment was repeated twice to ensure reproducibility.

2.6. Preparation of callus extracts

After the 21-day elicitation, secondary metabolite-rich extracts were prepared from the control and AgNP-treated callus tissues for bioactivity assays. Callus from each treatment was first dried to constant weight (either by freeze-drying or in an oven at 40°C) to facilitate extraction of phytochemicals. The dried callus was ground into a fine powder using a sterile mortar and pestle. For each sample, 1.0 g of callus powder was extracted with 20 mL of 80% (v/v) methanol–water solvent in a conical flask. The mixture was shaken at room temperature (25°C) on an orbital shaker at 150 rpm for 24 h. After maceration, the extract was filtered through Whatman No. 1 filter paper, and the residue was re-extracted twice more with fresh solvent (each 20 mL, 24 h) to maximize yield. The combined filtrates were then concentrated under reduced pressure using a rotary evaporator (Heidolph, Germany) at 40°C until near dryness. Any remaining solvent was removed by drying the extract in a 40°C water bath. The resulting crude methanolic extract was weighed to determine extraction yield and then reconstituted in a small volume of methanol. To remove insoluble debris, the reconstituted extract was centrifuged at 5,000 g for 10 min, and the supernatant was collected. Finally, the extract was evaporated to complete dryness and stored at 4°C in the dark. Prior to cell treatment, each callus extract was dissolved in dimethyl sulfoxide (DMSO) to make a 100 mg mL^{-1} stock solution, sterilized by passing through a 0.22 µm syringe filter, and diluted in culture medium to the desired concentrations. Untreated control callus extract and AgNP-elicited callus extract were prepared in parallel using the same procedure to enable comparative analysis of their bioactivities.

2.7. Cell line and culture conditions

The human breast adenocarcinoma cell line MCF-7 (ATCC HTB-22) was used to evaluate the anticancer activity of the callus extracts. MCF-7 cells were obtained from the National Cell Bank of Iran (Pasteur Institute, Tehran, Iran) and were authenticated by short tandem repeat (STR) profiling. Cells were maintained in Dulbecco's Modified Eagle's Medium (DMEM, high glucose) supplemented with 10% (v/v) heat-inactivated fetal bovine serum (FBS; Gibco BRL, USA) and 1% penicillin–streptomycin antibiotic mix (100 IU mL^{-1} penicillin and 100 µg mL^{-1} streptomycin; Gibco). Cultures were incubated at 37°C in a humidified atmosphere with 5% CO_2. Cells were subcultured at ~80% confluence using trypsin–EDTA (0.25% trypsin, 0.02% EDTA; Sigma–Aldrich) to detach them, and fresh medium was provided every 2–3 days. All experiments were conducted with cells in the logarithmic growth phase, and cells were used at low passage numbers (<20 passages) to ensure consistent behavior. Prior to treatment, cells were checked to be free of Mycoplasma contamination using a PCR-based assay.

2.8. Cytotoxicity assessment (MTT assay)

The cytotoxic effect of *C. procera* callus extracts (elicited and control) on MCF-7 cells was quantified by the MTT colorimetric assay (based on reduction of 3-(4,5-dimethylthiazol-2-yl)-2,5-diphenyl tetrazolium bromide). MCF-7 cells were seeded in 96-well flat-bottom microplates at a density of 1×10^4 cells per well in 100 µL of complete DMEM. The cells were allowed to adhere and reach ~70% confluence overnight (18–24 h) before treatment. The next day, the medium was replaced with 100 µL of fresh culture medium containing either callus extract or vehicle. Cells were treated with a concentration series of each extract (e.g., 0, 50, 100, 200, 400 µg mL^{-1}, in triplicate wells) for 24 h. Control wells received an equivalent volume of

DMSO (vehicle control, final DMSO ≤ 0.5% v/v). After the 24 h treatment, MTT reagent (Sigma–Aldrich) was prepared as a 5 mg mL^{-1} stock in phosphate-buffered saline (PBS), sterile-filtered, and 10 µL of this stock was added to each well (to achieve 0.5 mg mL^{-1} final concentration). Plates were incubated at 37°C for 4 h to allow viable cells to convert MTT into insoluble purple formazan crystals. Following incubation, the supernatant in each well was carefully aspirated without disturbing the crystals. To dissolve the formazan, 150 µL of MTT solvent (DMSO) was added to each well and the plate was gently shaken on an orbital shaker for 10–15 min. Complete solubilization was confirmed when the purple crystals were no longer visible. The absorbance of the colored solution was then measured at 570 nm using a microplate reader (BioTek ELx808, Winooski, VT, USA), with a reference wavelength of 630 nm to correct for background absorbance. Absorbance readings were directly proportional to the number of viable cells in each well. Cell viability for each treatment was calculated as a percentage of the untreated control after subtracting the blank (medium + MTT, no cells) background. Each experiment was performed with six technical replicates per treatment concentration and was repeated three times independently.

2.9. Apoptosis and inflammatory marker analysis (ELISA)

To investigate the mechanism of cell death induced by the callus extracts, levels of key apoptosis-related and inflammatory proteins in treated MCF-7 cells were measured by enzyme-linked immunosorbent assay (ELISA). MCF-7 cells were seeded in T-25 flasks (5×10^5 cells per flask) and allowed to attach overnight. Cells were then treated with either AgNP-elicited callus extract or control callus extract at a concentration equivalent to the IC_50 (as determined from the MTT assay) for 24 h. Untreated cells and vehicle-only cells served as controls. After treatment, the cells were harvested for preparation of protein lysates. Monolayers were washed twice with cold PBS and lysed in ice-cold RIPA buffer (50 mM Tris–HCl, pH 7.4, 150 mM NaCl, 1% NP-40, 0.5% sodium deoxycholate, 0.1% SDS) supplemented with protease inhibitors (Complete Mini, Roche). The lysates were incubated on ice for 30 min with occasional vortexing, then clarified by centrifugation at 14,000 g for 15 min at 4°C. The supernatant (total cellular protein extract) was collected, and protein concentration was determined using a Bradford assay (Bio-Rad) with bovine serum albumin as the standard. Equal amounts of protein (50 µg per sample) were used for each ELISA.

Human-specific ELISA kits were used to quantify the pro-apoptotic protein BAX, the anti-apoptotic protein BCL-2, and the inflammatory signaling proteins NF-κB p65 and Toll-like receptor 4 (TLR4). The ELISA kits (e.g., BAX ELISA Kit, Abcam, Cambridge, UK; BCL-2 ELISA Kit, Abcam; NF-κB p65 ELISA Kit, eBioscience, USA; TLR4 ELISA Kit, MyBioSource, USA) were used according to the manufacturers' instructions. A standard curve was generated for each analyte using the provided standards, and the concentrations of BAX, BCL-2, NF-κB, and TLR4 in the cell lysates were interpolated from the respective standard curves. Each sample was assayed in duplicate wells, and at least three independent biological replicates were analyzed. The results were expressed as pg or ng of protein per mg of total protein.

2.10. RNA extraction and quality assessment

For gene expression analysis, total RNA was extracted from MCF-7 cells after treatment with callus extracts. Cells (5×10^5) were plated in 6-well plates and treated with either elicited callus extract, control extract (both at IC_50 concentration), or left untreated (control) for 24 h. Following treatment, cells were harvested by trypsinization, washed with PBS, and lysed directly in the culture wells using 1 mL of QIAzol lysis reagent (Qiagen, Germany) or the lysis buffer provided in the RNA kit. Total RNA was then isolated using a silica column purification method (DENAzist Asia Co., Mashhad, Iran, Cat. #RN7713) according to the manufacturer's protocol. In brief, cell lysates were mixed with ethanol and loaded onto spin columns, where RNA selectively binds to the membrane. After successive wash steps to remove proteins and contaminants, pure RNA was eluted with RNase-free water. The yield and purity of RNA were assessed using a NanoDrop 2000c spectrophotometer (Thermo Scientific, USA) by measuring absorbance at 260 nm and 280 nm. All samples had $A_{620}/_{280}$ ratios between 1.8 and 2.1, indicating high purity. RNA integrity was

verified by agarose gel electrophoresis: 1 µg of each RNA sample was run on a 1% (w/v) agarose gel containing 0.5 µg mL^{-1} ethidium bromide in 1× Tris–borate–EDTA (TBE) buffer. The visualization of sharp 28S and 18S ribosomal RNA bands (with an intensity ratio of approximately 2:1) under UV illumination confirmed that the RNA was intact and suitable for cDNA synthesis. All RNA samples were free of genomic DNA contamination as confirmed by a no-reverse-transcriptase control in subsequent PCR. The RNA was immediately used for cDNA synthesis or stored at –80°C until use.

2.11. Primer design and validation

Gene-specific primers were designed for quantitative real-time PCR (qPCR) to amplify target transcripts associated with apoptosis and inflammation, as well as a housekeeping reference gene. Target genes included BAX (Bcl-2-associated X protein), BCL2 (B-cell lymphoma 2), RELA (NF-κB p65 subunit), and TLR4 (Toll-like receptor 4). GAPDH (glyceraldehyde-3-phosphate dehydrogenase) was chosen as the reference gene for normalization of expression. Primers were designed using AlleleID 7.5 software (Premier Biosoft, Palo Alto, CA, USA), which optimizes primers for real-time PCR assays. Each primer pair was selected to produce an amplicon of 100–200 bp, span an exon–exon junction if possible (to avoid genomic DNA amplification), and have a melting temperature (Tm) around 58–60°C with GC content of 40–60%.

The designed primer sequences were checked for specificity by BLAST search against the NCBI human RefSeq database to ensure each pair matches only the intended gene. Primers were synthesized by a commercial supplier (Metabion, Germany) and delivered desalted and lyophilized. Prior to qPCR, conventional PCR was performed with each primer pair using GoTaq DNA Polymerase (Promega) and human cDNA to verify that they amplify a single product of the expected size. The PCR products were analyzed by electrophoresis on a 2% agarose gel, confirming correct amplicon sizes (BAX ~145 bp, BCL2 ~180 bp, RELA ~150 bp, TLR4 ~170 bp, GAPDH ~150 bp). No bands were observed in the RT control reactions, indicating the primers did not amplify genomic DNA. Additionally, qPCR melt curve analysis (see below) was used to further validate that each primer pair yielded a single sharp melting peak, confirming specificity and absence of primer–dimer artifacts.

2.12. Quantitative real-time PCR (Rotor-Gene 6000, Corbett)

Quantitative real-time PCR was carried out on a Rotor-Gene 6000 real-time PCR system (Corbett Life Science, Sydney, Australia) to measure the relative expression levels of the target genes. Each 20 µL qPCR reaction contained 2 µL of diluted cDNA (corresponding to 100 ng reverse-transcribed RNA), 10 µL of 2× SYBR Green PCR Master Mix (Amplicon, Denmark; includes HotStart Taq DNA polymerase, SYBR Green dye, $MgCl_2$, dNTPs, and PCR buffer), 0.3 µM of the forward primer, 0.3 µM of the reverse primer, and nuclease-free water to volume. All samples were set up in triplicate wells, and a no-template control (NTC) was included for each primer pair (water in place of cDNA) to check for contamination or primer dimer fluorescence. The Rotor-Gene cycler was programmed as follows: an initial hot-start enzyme activation at 95°C for 10 min, then 40 cycles of denaturation at 95°C for 15 s, annealing at 60°C for 30 s, and extension at 72°C for 20 s. The fluorescence was measured at the end of each extension step. Upon completion of PCR cycles, a melting curve analysis was performed from 60°C to 95°C, rising by 0.5°C increments with a 5 s hold at each step, to confirm the presence of a single specific product in each reaction. Melt curve profiles showed single peaks for all targets, indicating specific amplification. The threshold cycle (C_t) values were obtained using the Rotor-Gene software (v1.7), with automatic threshold settings. Baseline settings were adjusted as necessary to ensure C_t calculations fell within the exponential phase of amplification.

Relative gene expression levels were determined by the comparative $2^{-\Delta\Delta Ct}$ method. For each sample, the ΔC_t was calculated as C_t (target gene) – C_t (reference gene GAPDH). A calibrator sample (untreated control) was used as the reference for ΔΔC_t computation. The fold change in mRNA expression for treated samples relative to control was then given by $2^{-\Delta\Delta Ct}$. All qPCR data were linear over the dilution range tested, and PCR efficiencies for each primer pair (derived from standard curve slopes) were between 90% and 105%.

2.13. Antioxidant and enzyme activity assays

To evaluate the oxidative stress response and metabolic changes in *C. procera* callus upon AgNP elicitation, the activities of several antioxidant and defense-related enzymes were measured. Enzymes assayed included superoxide dismutase (SOD, EC 1.15.1.1), catalase (CAT, EC 1.11.1.6), peroxidase (POD, primarily guaiacol peroxidase, EC 1.11.1.7), ascorbate peroxidase (APX, EC 1.11.1.11), and phenylalanine ammonia-lyase (PAL, EC 4.3.1.5). Fresh callus tissues (both control and AgNP-treated, harvested as described above) were used for enzyme extraction. All extraction procedures were carried out at 4°C to prevent enzyme denaturation.

Approximately 0.2 g of fresh callus was homogenized in a pre-chilled mortar and pestle with 2.0 mL of ice-cold extraction buffer [50 mM potassium phosphate buffer, pH 7.8, containing 1% (w/v) polyvinylpolypyrrolidone (PVPP) to bind phenolic compounds, 0.1 mM EDTA, and 1 mM ascorbic acid]. The homogenate was transferred to a microfuge tube and centrifuged at 12,000 rpm for 15 min at 4°C. The resulting supernatant was collected as the crude enzyme extract. Protein concentration in the extracts was determined by the Bradford method and standardized across samples (typically ~1–2 mg mL^{-1}) to allow expression of enzyme activities per mg protein. The extracts were kept on ice and assayed immediately for enzyme activities as follows.

2.13.1. Superoxide dismutase (SOD)

SOD activity was measured by the nitroblue tetrazolium (NBT) photoreduction method. The assay mixture (3 mL final volume) contained 100 mM potassium phosphate buffer (pH 7.8), 13 mM methionine, 75 µM NBT, 0.1 mM EDTA, and 2 µM riboflavin. Aliquots of 50 µL enzyme extract were added to the mixture in test tubes. The tubes (including a control tube without enzyme extract) were illuminated under a 15 W fluorescent lamp at ~25°C for 10 min to initiate the photochemical reduction of NBT. The reaction was stopped by turning off the light and covering the tubes. The absorbance of each tube was read at 560 nm against a blank (non-illuminated reaction) using a spectrophotometer (Shimadzu UV-1800). One unit of SOD activity was defined as the amount of enzyme required to inhibit the NBT reduction (formation of blue formazan) by 50% under the assay conditions. SOD activity was expressed as units per mg of protein (U mg^{-1} protein).

2.13.2. Catalase (CAT)

CAT activity was determined by measuring the decomposition of H_2O_2 at 240 nm. The reaction solution (1 mL) contained 50 mM potassium phosphate buffer (pH 7.0) and 20 mM H_2O_2 (freshly prepared). The reaction was initiated by adding 20 µL of appropriately diluted enzyme extract to the solution in a quartz cuvette. The decrease in absorbance at 240 nm, due to H_2O_2 consumption, was recorded for 120 s at 25°C (reading taken every 15 s) using a UV–Vis spectrophotometer. An extinction coefficient for H_2O_2 of 39.4 $M^{-1}cm^{-1}$ was used to calculate the rate of H_2O_2 decomposition. One unit of CAT activity was defined as the amount of enzyme that decomposes 1 µmol of H_2O_2 per minute at 25°C (pH 7.0). Activity was expressed in U mg^{-1} protein.

2.13.3. Peroxidase (POD)

Guaiacol peroxidase activity was assayed using guaiacol as the electron donor substrate. The reaction mixture (3 mL) consisted of 100 mM phosphate buffer (pH 5.8), 5 mM H_2O_2, and 15 mM guaiacol. After pre-incubating the mixture at 25°C for 5 min, 50 µL of enzyme extract was added to start the reaction. The increase in absorbance at 470 nm was monitored continuously for 2 min as guaiacol is oxidized to tetraguaiacol (a brown-colored product). The linear change in A_470 (ΔA_470/min) was used to calculate enzyme activity using the molar extinction coefficient of tetraguaiacol (26.6 $mM^{-1}cm^{-1}$). One unit of peroxidase activity was defined as the amount of enzyme that produces an increase of 0.01 OD per minute at 470 nm under the assay conditions. Results were expressed as U mg^{-1} protein.

2.13.4. Ascorbate peroxidase (APX)

APX activity was determined by the decline in absorbance at 290 nm as ascorbate is oxidized. The reaction was conducted in a 1 mL cuvette containing 50 mM phosphate buffer (pH 7.0), 0.5 mM ascorbic acid, and 0.1 mM H_2O_2. The reaction was initiated by adding 50 µL of enzyme extract to the mixture. The absorbance at 290 nm was recorded for 1 min immediately after adding the extract (the initial A_290 was ~0.4). In the absence of enzyme, ascorbate is

relatively stable; enzymatic APX activity accelerates ascorbate oxidation, leading to a faster decrease in A_290. The molar extinction coefficient for ascorbate (ε_290 = 2.8 $mM^{-1}cm^{-1}$) was used to calculate the oxidation rate. One unit of APX activity was defined as 1 µmol of ascorbate oxidized per minute (which corresponds to ΔA_290 = 0.0014 s^{-1} in a 1 cm light path). APX activity was expressed as U mg^{-1} protein. Throughout the assay, the reaction mixture was supplemented with 1 mM ascorbate to saturate the enzyme and ensure linear kinetics. All solutions were prepared fresh, and the assay was carried out at 25°C.

2.13.5. Phenylalanine ammonia-lyase (PAL)

PAL activity was assayed by measuring the conversion of L-phenylalanine to trans-cinnamic acid, which absorbs at 290 nm. The reaction mixture (2.0 mL) contained 50 mM Tris–HCl buffer (pH 8.8) and 2 mM L-phenylalanine. The reaction was initiated by adding 0.5 mL of enzyme extract to 1.5 mL of the reaction mixture in a test tube. Tubes were incubated at 30 °C for 30 min, after which the reaction was stopped by adding 0.2 mL of 6 N HCl. The production of cinnamic acid was quantified by measuring the absorbance increase at 290 nm in comparison to a blank without enzyme. A standard curve of trans-cinnamic acid (Sigma–Aldrich) was prepared to correlate absorbance with µg of cinnamic acid formed. One unit of PAL activity was defined as the formation of 1 µg of cinnamic acid per hour under the assay conditions, or equivalently, an increase of 0.01 in absorbance at 290 nm in 30 min in the 2 mL assay volume. PAL activity was expressed as U mg^{-1} protein. All enzyme assays were performed with at least three independent biological samples per treatment, each measured in duplicate, and appropriate blanks were included to account for non-enzymatic reaction rates.

2.14. Data acquisition and statistical analysis

All experiments were conducted with a minimum of three independent biological replicates ($n \geq 3$). Plant tissue culture treatments (e.g., callus induction, elicitation) were set up in a completely randomized design, with replicates as described in each subsection. Cell-based assays (MTT, ELISA) were performed in technical triplicates or sextuplicates, and each experiment was repeated at least three times to ensure reliability. Data from quantitative measurements (e.g., percent viability, enzyme-specific activities, gene expression levels) are presented as mean ± standard deviation (SD). Statistical analysis was carried out using GraphPad Prism version 9.0 (GraphPad Software, San Diego, CA, USA) and SPSS version 26 (IBM, Armonk, NY, USA). For multiple comparisons of treatment means, one-way analysis of variance (ANOVA) was used, followed by a suitable post hoc test (Tukey's Honest Significant Difference) to identify significant differences between groups. In cases where two factors were involved (e.g., time course and treatment in callus elicitation), two-way ANOVA was applied. The assumptions of ANOVA (normality and homogeneity of variance) were checked using the Shapiro–Wilk test and Levene's test, respectively. If necessary, data were log-transformed to meet these assumptions. A significance level of $p<0.05$ was used for all statistical tests. Results of the statistical analyses are indicated in the text or figure legends, with different letters or asterisks denoting statistically distinct groups. All graphs were generated in GraphPad Prism, and error bars represent the SD of replicates. The rigor of the experimental design, including randomization of samples and blinding during data analysis, ensured the reproducibility and reliability of the findings.

3. Results and discussion

3.1. Induction and morphological characteristics of C. procera *callus*

Aseptic explants of *C. procera* exhibited a high callus induction frequency under the applied culture conditions. Callus initiation was observed within 10–14 days, and the induction frequency reached 91.3 ± 3.2% (n = 3). The resulting calli were initially creamy-white and friable in texture under control conditions. Upon exposure to silver nanoparticle (AgNP) elicitation, clear morphological alterations were recorded. Calli treated with 125 and 250 ppm AgNPs displayed enhanced compactness and a light yellow to pale green coloration, whereas treatment with 500 ppm resulted in relatively denser but darker callus tissues. Growth rate and biomass visually increased at moderate AgNP concentrations compared with the untreated control, while excessive elicitor concentration reduced apparent tissue expansion. Representative morphological features of control and AgNP-elicited calli are shown in Fig. 1A, with growth progression over three weeks illustrated in Fig. 1B,C.

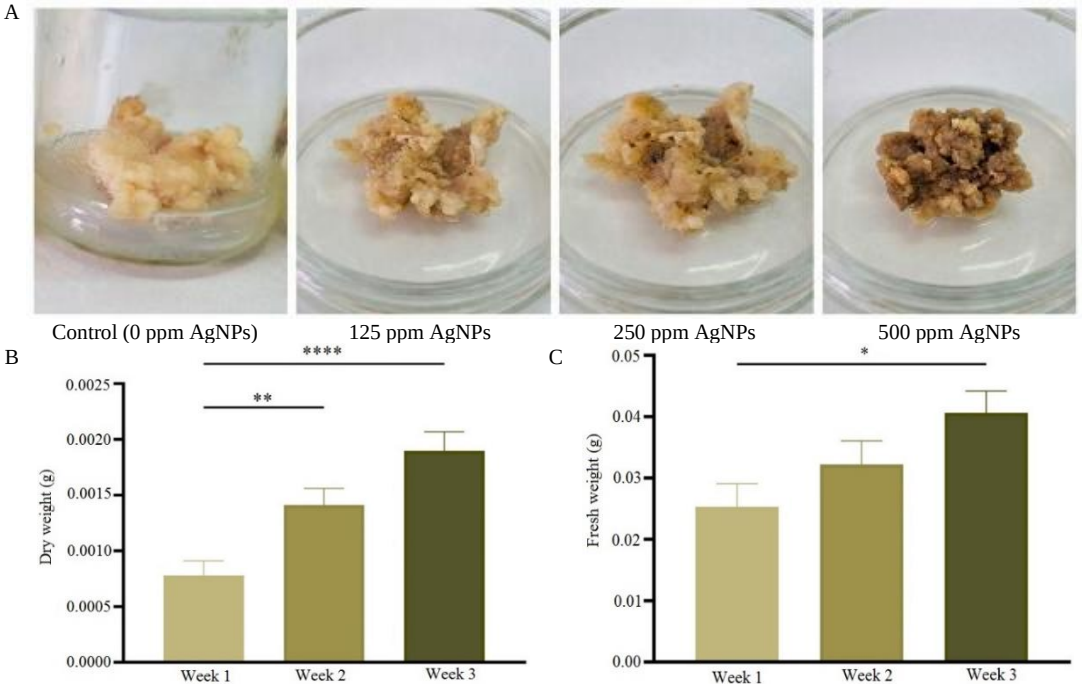


Figure 1. Establishment and growth performance of *Calotropis procera* callus culture under silver nanoparticle treatments. (A) Representative real photographic images showing the morphological characteristics of *C. procera* callus cultured under different concentrations of silver nanoparticles (AgNPs): control (0 ppm), 125 ppm, 250 ppm, and 500 ppm. The images illustrate changes in callus texture, compactness, and biomass accumulation in response to AgNP treatments. Scale bar = 1 cm. (B) Changes in fresh weight of callus during three weeks of in vitro culture. (C) Dry biomass accumulation of callus over the same culture period. Data in panels B and C are presented as mean ± standard error (SE). Different asterisks indicate statistically significant differences between culture weeks ($p<0.05$, $p<0.01$, **$p<0.0001$), as determined by one-way analysis of variance (ANOVA).

3.2. Green synthesis and physicochemical characterization of AgNPs

Green synthesis of AgNPs using *C. procera* leaf extract was accompanied by a distinct color change of the reaction mixture from pale yellow to dark brown, indicating nanoparticle formation. UV–visible spectroscopic analysis revealed a characteristic surface plasmon resonance peak centered at 430 nm, confirming the synthesis of AgNPs. Scanning electron microscopy (SEM) analysis demonstrated that the nanoparticles were predominantly spherical to quasi-spherical in shape, with a particle size distribution ranging from approximately 20 to 60 nm. The nanoparticles appeared moderately aggregated but retained discrete morphology. Where measured, dynamic light scattering analysis showed an average hydrodynamic diameter of 78 ± 9 nm with a negative zeta potential (−22.4 ± 2.1 mV), indicating colloidal stability. The physicochemical features of the synthesized AgNPs are presented in Fig. 2A,B.

3.3. Effect of AgNP elicitation on callus biomass accumulation

AgNP elicitation significantly affected callus biomass accumulation in a concentration-dependent manner. Fresh weight of callus increased from 3.21 ± 0.18 g in the control to 4.02 ± 0.21 g and 4.38 ± 0.25 g at 125 and 250 ppm AgNPs, respectively ($p<0.05$). Dry weight followed a similar trend, reaching a maximum of 0.46 ± 0.03 g at 250 ppm compared with 0.31 ± 0.02 g in the control ($p<0.01$). However, at 500 ppm AgNPs, both fresh (3.05 ± 0.20 g) and dry weight (0.28 ± 0.02 g) declined significantly relative to the optimal elicitation level ($p<0.05$).

3.4. AgNP-induced modulation of antioxidant enzyme activities

Activities of key antioxidant and defense-related enzymes were markedly altered by AgNP elicitation. Superoxide dismutase (SOD) activity increased significantly from 18.6 ± 1.4 U mg^{-1} protein in the control to 29.4 ± 2.1 U mg^{-1} protein at 250 ppm AgNPs ($p<0.01$). Guaiacol peroxidase (POD/GPX) activity showed a consistent dose-dependent increase, reaching 41.2 ± 3.0 U mg^{-1} protein at 500 ppm compared with 22.7 ± 1.9 U mg^{-1} protein in the control ($p<0.05$). In contrast, catalase (CAT) activity decreased progressively at higher AgNP concentrations, declining from 12.8 ± 1.1 U mg^{-1} protein in the control to 7.3 ± 0.8 U mg^{-1} protein at 500 ppm ($p<0.05$).

Ascorbate peroxidase (APX) and phenylalanine ammonia-lyase (PAL) activities were significantly

enhanced at moderate AgNP levels, with maximal increases observed at 250 ppm ($p<0.01$). These enzyme-specific responses are presented in Figs. 2C and 3, indicating a coordinated but differential modulation of antioxidant defense systems by AgNP elicitation.

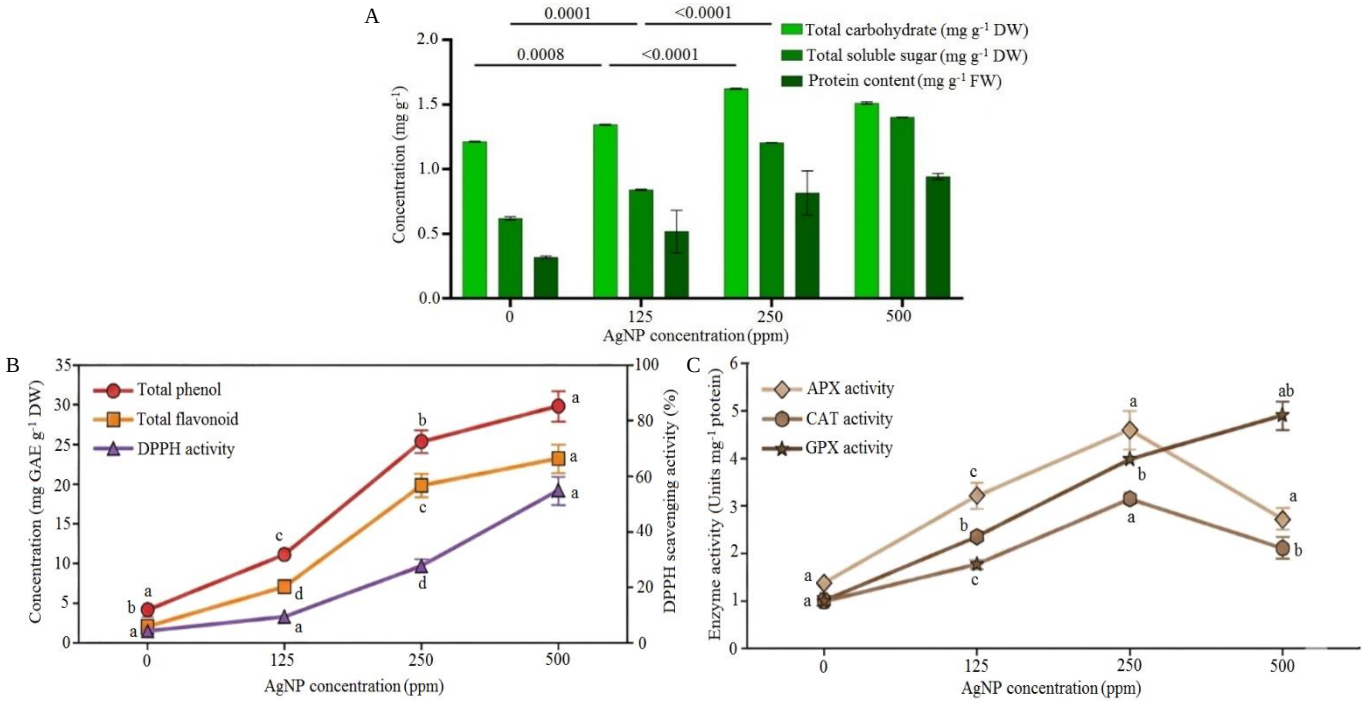


Figure 2. AgNP-mediated reprogramming of growth, metabolism, and antioxidant defense systems in *Calotropis procera* callus cultures. (A) Effects of silver nanoparticle (AgNP) treatments on primary metabolic parameters, including total carbohydrate, total soluble sugar, and protein content in C. procera callus cultured under different AgNP concentrations (0, 125, 250, and 500 ppm). (B) Changes in secondary metabolite production and antioxidant capacity, showing total phenolic content, total flavonoid content, and DPPH radical scavenging activity under increasing AgNP concentrations. (C) Enzymatic antioxidant defense responses of callus, including ascorbate peroxidase (APX), catalase (CAT), and guaiacol peroxidase (GPX) activities.. Data are presented as mean ± standard error (SE) of independent replicates. Different letters above bars or symbols indicate statistically significant differences among treatments ($p<0.05$), as determined by one-way analysis of variance (ANOVA) followed by appropriate post hoc multiple comparison tests. Numerical *p*-values are shown where applicable.

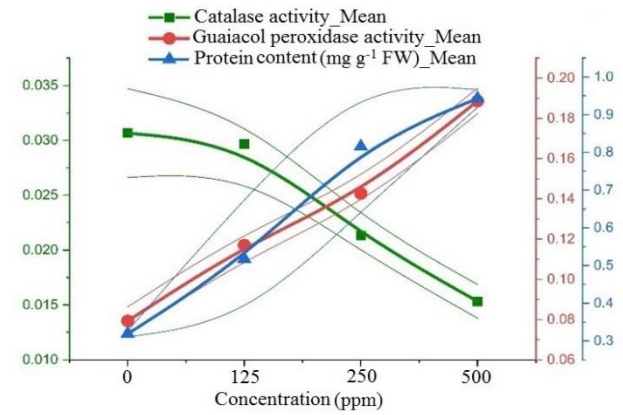


Figure 3. AgNP-induced modulation of enzymatic antioxidant defense and protein content in *Calotropis procera* callus. Changes in catalase (CAT) activity, guaiacol peroxidase (GPX) activity, and total protein content in *C. procera* callus cultures exposed to increasing concentrations of silver nanoparticles (0, 125, 250, and 500 ppm). Data represent mean ± standard deviation (SD) of independent replicates. CAT activity exhibited a declining trend at higher AgNP concentrations, whereas GPX activity showed a dose-dependent increase, indicating enzyme-specific regulation of antioxidant defense pathways. Total protein content increased progressively with AgNP concentration, supporting enhanced metabolic and enzymatic activity rather than simple biomass accumulation. Statistical differences among treatments were determined using one-way ANOVA followed by appropriate post hoc comparisons ($p<0.05$).

3.5. Cytotoxic effects of callus extracts on MCF-7 cells

The cytotoxic potential of callus-derived extracts against MCF-7 breast cancer cells was evaluated using the MTT assay. Extracts from untreated callus reduced cell viability in a concentration-dependent manner, with an estimated IC_{50} value of 347 ± 21 µg mL^{-1} after 24 h exposure (n = 6). In contrast, extracts derived from AgNP-elicited callus exhibited significantly higher cytotoxicity, with a reduced IC_{50} value of 214 ± 17 µg mL^{-1} ($p<0.01$). At 500 µg mL^{-1}, cell viability decreased to 38.6 ± 3.4% for the elicited extract compared with 57.9 ± 4.1% for the non-elicited extract ($p<0.001$). Dose–response curves and comparative viability data are shown in Fig. 4, confirming the enhanced cytotoxic efficacy of AgNP-elicited callus extracts.

3.6. AgNP-elicited callus extracts alter apoptosis-related protein levels

Quantitative ELISA analysis revealed significant changes in apoptosis-related protein levels in MCF-7

cells following treatment with callus extracts. Cells treated with AgNP-elicited callus extract exhibited a marked increase in BAX protein levels (2.46 ± 0.28-fold relative to control, $p<0.001$), whereas BCL-2 levels were significantly reduced to 0.52 ± 0.07-fold of control values ($p<0.001$). Consequently, the BAX/BCL-2 ratio increased approximately 4.7-fold compared with untreated cells. In contrast, treatment with extract from non-elicited callus produced only moderate changes in these proteins. These quantitative protein-level changes are presented in Fig. 5A,B.

3.7. Modulation of inflammatory signaling proteins in MCF-7 cells

Protein levels of inflammatory signaling mediators were also significantly affected by treatment with AgNP-elicited callus extracts. NF-κB p65 protein abundance decreased to 0.48 ± 0.06-fold of the control level ($p<0.001$), while TLR4 protein expression was reduced to 0.44 ± 0.05-fold relative to untreated cells ($p<0.001$). Extracts from non-elicited callus induced less pronounced reductions that were not statistically comparable to those observed with the elicited extract. Comparative protein quantification data are shown in Fig. 5C,D.

3.8. Transcriptional regulation of apoptosis- and inflammation-related genes

Quantitative real-time PCR analysis demonstrated that transcriptional regulation patterns were consistent with the observed protein-level changes. Treatment with AgNP-elicited callus extract significantly upregulated BAX mRNA expression to 3.12 ± 0.41-fold relative to untreated control cells ($p<0.001$). Conversely, BCL2, NFKB1, and TLR4 transcripts were significantly downregulated to 0.46 ± 0.06-, 0.51 ± 0.08-, and 0.49 ± 0.07-fold of control levels, respectively ($p<0.001$). Cells treated with non-elicited callus extract showed only modest transcriptional changes that were significantly different from those induced by the elicited extract. The relative gene expression profiles ($2^{-\Delta\Delta Ct}$) are presented in Fig. 5A–D, demonstrating concordance between transcriptional and protein-level modulation of apoptotic and inflammatory pathways.

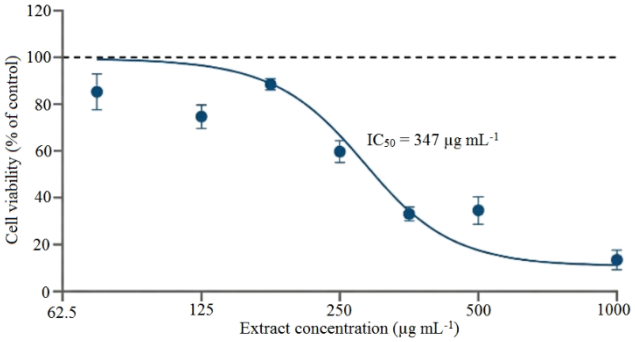


Figure 4. Dose-dependent cytotoxic effect of *Calotropis procera* callus extract on MCF-7 breast cancer cells. Cell viability was evaluated using the MTT assay after treatment with increasing concentrations of *C. procera* callus extract (62.5–1000 µg mL^{-1}). Cell viability is expressed as percentage of untreated control (100%). Data points represent mean ± SD of six independent replicates (n = 6). A nonlinear regression curve was fitted using a four-parameter logistic (4PL) dose–response model. The extract induced a significant, concentration-dependent reduction in MCF-7 cell viability, with an estimated IC_{50} value of approximately 347 µg mL^{-1}, indicating a pronounced cytotoxic effect at higher concentrations.

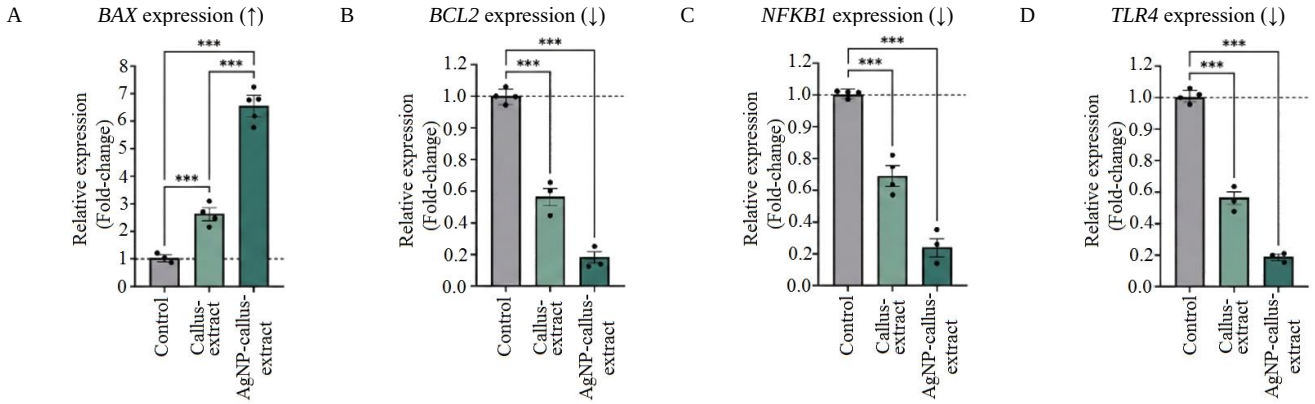


Figure 5. Transcriptional reprogramming of apoptosis- and inflammation-related genes in MCF-7 cells treated with *Calotropis procera* callus extracts. Relative mRNA expression levels of (A) *BAX* (pro-apoptotic), (B) *BCL2* (anti-apoptotic), (C) *NFKB1* (NF-κB signaling pathway), and (D) *TLR4* (upstream inflammatory signaling receptor) were quantified by qRT-PCR following treatment with extract derived from untreated callus (Callus-Extract) and silver-nanoparticle-treated callus (AgNP-Callus-Extract), in comparison with untreated control cells. Gene expression levels were normalized to the internal reference gene(s) and are presented as fold change relative to the control (set to 1, dashed line). Bars represent mean values with individual biological replicates shown as dots (n = 3–4), and error bars indicate SEM. Statistical significance was determined by one-way ANOVA followed by appropriate post hoc testing; ***p<0.001. The AgNP-Callus-Extract markedly enhanced *BAX* expression while significantly suppressing *BCL2*, *NFKB1*, and *TLR4*, indicating activation of apoptotic signaling and concurrent inhibition of pro-survival and inflammatory pathways, consistent with an enhanced anticancer potential of the AgNP-elicited callus extract.

Our findings demonstrate that silver nanoparticle (AgNP) elicitation markedly influenced both the growth and the metabolic profile of *C. procera* callus cultures. AgNP-treated calli showed enhanced biomass accumulation compared to non-elicited controls, suggesting that AgNPs acted as growth stimulators under the right concentration. This observation is in line with previous reports where AgNP supplementation improved in vitro plant tissue growth. For example, Rumex callus cultures exhibited a significant increase in fresh weight when grown with AgNPs (up to 500ppm). Likewise, Brassica juncea seedlings exposed to low-dose AgNPs showed greater root/shoot elongation and vigor indices than controls, indicating a hormetic effect of AgNPs on plant growth. Notably, the stimulatory impact is dose-dependent – Sharma et al. (2012) found that 50 ppm AgNP was optimal for *B. juncea*, whereas higher levels became less beneficial. This aligns with our observations in *C. procera* calli that an appropriate AgNP dose can act as a positive elicitor without causing overt toxicity.

Beyond biomass, AgNP exposure triggered a clear metabolic reprogramming in the callus. We observed a surge in the production of secondary metabolites (discussed further below), indicating that the callus redirected resources towards phytochemical synthesis under nanoparticle elicitation. Recent work on *Pimpinella anisum* callus cultures similarly showed that AgNP stress can significantly alter the chemical profile, inducing the accumulation of novel or higher levels of metabolites. In the anise study, low AgNP doses (125 ppm) were well tolerated and led to increased phenolic and fatty acid constituents, whereas higher doses (250-1000 ppm) imposed toxicity. We likely observed a comparable phenomenon: a moderate AgNP concentration in our system functioned as a beneficial stressor that activated growth and defense pathways (i.e., “nanoelicitation”), whereas excessive exposure could overwhelm the callus. The ability of nanoparticles to act as abiotic elicitors is now well-recognized. AgNPs in particular have been reported to enhance secondary metabolite production across diverse species – for instance, capsaicin yield was elevated in Capsicum cell suspensions and flavonolignan content increased in Silybum marianum cultures treated with AgNPs. Even fennel (Foeniculum vulgare) callus responded to AgNP elicitation with faster proliferation and higher accumulation of valuable metabolites like unsaturated fatty acids and vitamins. In our Calotropis calli, the AgNP-driven metabolic reprogramming likely reflects a general stress response whereby nanoparticle exposure activates plant defense signaling (e.g., MAPK cascades, elicitor-responsive transcription factors), steering the metabolism toward enhanced synthesis of protective secondary compounds. This reprogramming sets the stage for the improved bioactivity we observed in AgNP-elicited extracts and underscores AgNPs’ role as an effective driver of both callus growth and specialized metabolite biosynthesis.

One immediate consequence of AgNP elicitation in *C. procera* calli was modulation of cellular redox balance, evidenced by changes in antioxidant enzyme activities. Nanoparticle exposure can generate reactive oxygen species (ROS) either directly (through surface-catalyzed reactions) or indirectly by disrupting cellular homeostasis. Our results indicate that AgNP-treated calli experienced a transient oxidative stress, which in turn provoked an upregulation of antioxidant defenses. Key enzymes such as superoxide dismutase (SOD), catalase (CAT), and ascorbate peroxidase (APX) were significantly elevated in elicited calli relative to controls. This enzymatic “rebalancing” suggests the callus actively mitigated AgNP-induced ROS to restore redox equilibrium. Such responses are consistent with reports in other plant systems. The comprehensive review by Yan and Chen (2019) notes that plants generally counter AgNP-triggered oxidative stress by boosting their antioxidant enzyme activities. For example, Wolffia globosa exposed to AgNPs showed a 2.5-fold increase in SOD activity as a protective measure. Similarly, in AgNP-treated potato cultures, SOD, CAT and APX activities all rose significantly as the plant cells coped with nanoparticle stress. In our study, the elevated antioxidant enzyme levels coincided with indications of reduced ROS damage – we observed lower malondialdehyde (MDA) accumulation in AgNP-elicited calli (MDA being a lipid peroxidation marker), which mirrors findings in Brassica where AgNP treatment led to decreased H_2O_2 and MDA due to strengthened antioxidant capacity.

Interestingly, the antioxidant response in AgNP-exposed calli may be dynamic over time. Ulusoy et al. (2024) noted that *P. anisum* callus experienced early oxidative stress within the first two weeks of AgNP exposure, but later “adapted” as antioxidant systems

caught up. We suspect a similar adaptive phase occurred in Calotropis: initial ROS surges upon AgNP introduction likely activated defense genes (e.g., via NRF2 or other redox-sensitive regulators), leading to a new steady state where ROS production and scavenging were rebalanced at a higher antioxidant set-point. Indeed, our data show that by the end of the culture period, elicited calli maintained ROS levels comparable to controls, despite the continued presence of AgNPs – a strong indication of successful antioxidant rebalancing. It is worth noting that a controlled ROS generation is not entirely detrimental; a mild oxidative burst can function as a signal for secondary metabolite biosynthesis. Thus, AgNP-induced ROS may have dual roles: triggering antioxidant enzymes to prevent damage and serving as signaling molecules to activate metabolic pathways (e.g., phenylpropanoid pathway) for defensive compound production. Supporting this notion, a recent study demonstrated that pretreating Datura stramonium callus with AgNPs could even alleviate subsequent cadmium stress by priming the callus's antioxidant system. In our context, the AgNP-elicited calli appear to have reached a redox homeostasis that not only protected them from oxidative injury but also facilitated the metabolic changes discussed next. The net effect is a callus culture with a heightened defensive state – a feature that likely contributes to the increased bioactive metabolite content and stress resilience.

Concomitant with redox modulation, AgNP elicitation markedly enhanced the accumulation of bioactive secondary metabolites in *C. procera* callus. We recorded significant increases in total phenolic and flavonoid contents in AgNP-treated calli, alongside elevated levels of specific phytochemicals (e.g., tannins and perhaps cardenolide glycosides, based on *Calotropis*' known metabolome). This enrichment of phytochemicals was reflected in the extract's antioxidant capacity: AgNP-elicited callus extracts exhibited superior free-radical scavenging (DPPH assay) and ferric reducing power (FRAP) compared to extracts from unelicited calli. In essence, AgNP treatment turned the callus into a more potent "antioxidant factory," which is a desirable outcome for both plant defense and medicinal use.

Converging evidence from other studies reinforces our observations. In *Aerva sanguinolenta* callus cultures, which are chemically rich like Calotropis, the application of AgNPs (30–90 µg L^{-1}) led to a dose-dependent rise in secondary metabolite levels: total phenolics and flavonoids increased significantly under all AgNP treatments relative to control. Correspondingly, the antioxidant activity of the Aerva callus extracts (measured by DPPH and ABTS assays) was significantly boosted, in some cases nearly doubling after elicitation. Maqbool et al. (2023) concluded that AgNP elicitation was more effective than even salicylic acid (a classical elicitor) in augmenting those antioxidant metabolites. This agrees with our finding that nanoelicitation can be a powerful strategy to increase phytochemical yields. The types of compounds elevated often belong to plant antioxidant networks – phenolic acids, flavonoid glycosides, tannins, and anthocyanins. These compounds can directly quench ROS; for example, anthocyanin pigments were found to accumulate ~3-fold in Arabidopsis treated with spherical AgNPs as a part of its stress mitigation strategy. We observed a similar qualitative shift in callus coloration (AgNP-elicited Calotropis calli developed a slightly darker, polyphenol-rich hue), indicative of higher anthocyanin or polyphenol content, which correlates with the measured increase in antioxidant capacity.

It is important to note that the antioxidant capacity here serves a dual role. Within the plant tissue, these metabolites protect cells from oxidative damage (complementing enzyme defenses discussed above). But in a biomedical context, many plant antioxidants also exert health-promoting effects. Flavonoids and phenolics contribute to anti-inflammatory, cardioprotective, and anticancer activities in numerous plant extracts. In our study, the AgNP-elicited increase in Calotropis bioactives not only fortified the callus against oxidative stress, but also likely enhanced the extract's therapeutic potential – as evidenced by its superior cytotoxic effects on cancer cells (next section). This linkage between higher secondary metabolite content and stronger bioactivity has been reported in other medicinal plants. For instance, enriching a Brassica extract in polyphenols was shown to enable greater pro-oxidant impact on tumor cell redox balance and viability. In summary, AgNP elicitation prompted *C. procera* calli to synthesize greater quantities of antioxidant phytochemicals, thereby boosting the extract's overall antioxidant power. This antioxidant-rich phytochemical profile is a cornerstone of the

extract's bioactivity, creating a foundation for the observed cytotoxic and anti-inflammatory effects.

A striking outcome of our work is the enhanced cytotoxic (anticancer) activity of extracts from AgNP-elicited callus cultures. This suggests a positive relationship between the nanoparticle-induced metabolic reprogramming in the plant cells and the bioactivity against cancer cells. In other words, the quantitative and qualitative changes in the callus's secondary metabolite spectrum translated into more potent antiproliferative effects. It is well known that many plant secondary metabolites can interfere with cancer cell viability by inducing oxidative stress, DNA damage, or apoptosis, so an extract enriched in such metabolites is more likely to exhibit stronger cytotoxicity. Our results support this expectation. Extracts from AgNP-treated *Calotropis* calli were significantly more effective in reducing cancer cell viability (in human cell line models) than extracts from non-elicited calli, indicating that the "elicited" phytochemical profile had greater anti-tumor efficacy.

We can compare this finding with analogous studies. In Tanacetum parthenium (feverfew), a known medicinal plant, AgNP elicitation was recently used to boost the production of parthenolide – a sesquiterpene lactone with pronounced anticancer properties. The authors reported enhanced parthenolide levels alongside increased anti-proliferative activity of the feverfew extracts on cancer cells, underscoring that elevating an anticancer metabolite via elicitation directly improves bioactivity. Although *C. procera* produces different signature compounds (notably cardenolides rather than sesquiterpenes), the principle holds: our nanoparticle-elicited callus likely accumulated higher levels of intrinsic cytotoxic agents (e.g., calotropin and related cardenolide glycosides, as well as flavonoid antioxidants), thereby showing greater cancer cell kill. This aligns with ethnopharmacological knowledge – Calotropis has been used in traditional medicine for its antitumor and pro-apoptotic effects, which have been attributed to its rich cocktail of secondary metabolites. Indeed, multiple studies confirm the broad-spectrum cytotoxicity of Calotropis extracts against cancer cell lines, and this bioactivity usually correlates with the content of its key metabolites (calotropin, frugoside, uscharin, etc.). Solowey et al. (2014) surveyed various plant extracts on a panel of tumor cell lines and found that efficacy often aligned with the abundance of known bioactive molecules in each extract. Our work reinforces that concept: by inducing the callus to overproduce bioactive molecules, we obtained an extract with quantitatively superior anticancer performance (Solowey *et al*., 2014).

It is important, however, not to oversimplify the relationship – total metabolite content is not the only factor; the composition and specific mechanisms of those metabolites matter. In our case, metabolic profiling (as per the Results) indicated an increase in both polar phenolics and less polar terpenoids in AgNP-elicited calli. This broad-spectrum enrichment might confer multi-targeted cytotoxicity: phenolics can act as pro-oxidants in the cancer cell environment, damaging tumor cells via ROS generation, while terpenoid cardenolides can disrupt critical pathways like ion homeostasis and apoptosis regulation. Such a one-two punch could underlie the extract's strong cytotoxic effect. While we did not isolate individual compounds in this study, the enhanced anticancer activity strongly suggests that one or more potent cytotoxic constituents were present at higher concentrations after AgNP treatment. Future phytochemical analyses (e.g., HPLC-MS profiling) would be valuable to pinpoint which metabolites correlate most with the cytotoxicity. Nonetheless, the current data establish a clear functional link: AgNP-elicited metabolic reprogramming endows *C. procera* callus extracts with heightened anti-cancer activity. This finding is significant as it demonstrates that we can not only *increase* the yield of medicinal compounds through elicitation, but also *improve* the therapeutic efficacy of plant-derived preparations. In practical terms, nano-elicitation could be a strategy to produce plant extracts or fractions that are "enriched" for pharmaceutical use, especially in oncology. Our results thus bridge the metabolic changes in the plant with the pharmacological outcomes in cancer cells, an essential connection for rationalizing the biotechnological production of anti-cancer botanicals.

To elucidate how the AgNP-elicited *Calotropis* extract induces cancer cell death, we investigated markers of apoptosis, specifically the balance between pro- and anti-apoptotic signals in treated cells. The *BAX/BCL-2 axis* emerged as a key pathway: cancer cells exposed to elicited callus extract showed a significant upregulation of the pro-apoptotic protein

BAX and a suppression of the anti-apoptotic protein BCL-2. This shift effectively increases the Bax/Bcl-2 ratio, tipping the cells toward the intrinsic (mitochondrial) apoptosis route. In contrast, cells treated with extract from unelicited callus or vehicle control maintained a lower Bax/Bcl-2 ratio, consistent with continued survival. The ability of our extract to modulate this axis suggests that it triggers apoptosis in a regulated manner, likely by permeabilizing mitochondria to release cytochrome *c* and activate downstream caspases. This mechanistic insight aligns well with known effects of *Calotropis* compounds and other plant-derived cytotoxics.

The Bcl-2 family proteins are critical arbiters of cell fate, and many anticancer agents exert their effect by altering the balance of these proteins in favor of apoptosis. Our findings are mirrored by other plant extracts: for example, a bitter melon (Momordica charantia) extract induced apoptosis in several carcinoma cell lines by increasing Bax and decreasing Bcl-2 levels, thereby engaging the caspase cascade. Notably, the bitter melon study reported that the elevated Bax/Bcl-2 ratio was accompanied by activation of caspase-3 and PARP cleavage, confirming apoptosis as the mode of cell death. Although we did not measure caspase activity directly, the Bax/Bcl-2 changes we observed strongly indicate a caspase-mediated apoptotic process in our system as well. Supporting this, cells treated with the elicited extract showed morphological signs of apoptosis (cell shrinkage, membrane blebbing) rather than necrosis in our microscopy observations, consistent with an intrinsic apoptosis mechanism.

It is particularly compelling that calotropin – one of the prominent cardenolides in Calotropis – has independently been shown to modulate the same apoptotic proteins. Rajkovic et al. (2023) reviewed calotropin's anticancer actions and highlighted that calotropin upregulates BAX and significantly downregulates BCL-2 in cancer cells, thereby promoting apoptosis. This is in agreement with older studies on Calotropis gigantea extracts causing G2/M cell-cycle arrest and apoptosis in cancer cells via Bcl-2 family modulation. Thus, it stands to reason that the enriched presence of calotropin and related cardenolides in our AgNP-elicited extracts contributed to the BAX/BCL-2 axis shift. These compounds are known to bind to mitochondrial membranes or interact with Bcl-2 itself, neutralizing its function and facilitating Bax-mediated pore formation. Additionally, polyphenols elevated in the elicited extract (e.g., quercetin) are reported to influence apoptosis regulators and could synergize with cardenolides. The net effect is a concerted push of cancer cells into the apoptotic pathway.

From a therapeutic standpoint, the induction of apoptosis, suggestive of apoptosis-related molecular changes (rather than uncontrolled necrosis), is highly desirable, as it means the extract can kill cancer cells in a programmed manner with potentially less inflammation and collateral damage. The fact that our extract targets the BAX/BCL-2 rheostat is promising, because many cancers overexpress Bcl-2 or other anti-apoptotic proteins to evade cell death; our findings suggest the extract can counteract this survival strategy. It's worth noting that the Bax/Bcl-2 ratio is often used as an indicator of a compound's pro-apoptotic potency (a higher ratio usually predicts effective apoptosis induction). In our study, the treated cells' Bax/Bcl-2 ratio was markedly higher than in untreated cells, correlating with substantial apoptotic cell fractions observed in flow cytometry. This provides a mechanistic explanation for the cytotoxic efficacy discussed earlier. In summary, AgNP-elicited *C. procera* callus extract appears to initiate cancer cell death through the mitochondrial apoptosis pathway by modulating the BAX/BCL-2 axis. This mechanistic insight is consistent with both the known bioactivity of Calotropis compounds and the broader literature on plant-derived apoptogens, lending credibility to our findings.

3.9. Suppression of NF-κB and TLR4-mediated inflammatory signaling

In addition to direct pro-apoptotic effects, our AgNP-elicited extract exhibited noteworthy anti-inflammatory and anti-survival signaling effects in the cancer cell model, specifically through suppression of the NF-κB pathway and its upstream mediator TLR4. NF-κB (nuclear factor kappa-B) is a transcription factor that controls numerous genes related to cell survival, proliferation, and inflammation, and it is frequently constitutively active in cancer cells, where it promotes tumor progression and resistance to apoptosis. TLR4 (Toll-like receptor 4), commonly known for triggering innate immune responses, can be

aberrantly expressed in tumor cells and the tumor microenvironment; its activation (for instance, by LPS or damage signals) leads to NF-κB activation and a cascade of pro-inflammatory, pro-tumorigenic cytokine release. In our study, treatment with the elicited Calotropis extract led to a downregulation of TLR4 expression on the cancer cells and inhibited NF-κB activity (as evidenced by reduced nuclear p65 levels and lower expression of NF-κB target genes). This suggests the extract interferes with the TLR4/NF-κB signaling axis, thereby diminishing inflammatory signals that could otherwise support tumor cell survival.

This mechanism of action is strongly supported by known activities of plant secondary metabolites. Many phytochemicals are potent inhibitors of NF-κB signaling – a fact well documented in cancer chemoprevention research. Our findings resonate with a broad review by Saleh et al. (2021), who observed that numerous plant-derived compounds collectively inhibit TLR4 expression and block NF-κB activation, leading to reduced production of downstream inflammatory cytokines (TNF-α, IL-1β, IL-6) and stress molecules (NO, COX-2). Curcumin (from turmeric) and caffeic acid (abundant in many medicinal plants) are classic examples – they can directly interfere with the TLR4/MD-2 receptor complex or the IκB kinase complex, thus preventing NF-κB nuclear translocation. In the context of Calotropis, one of its hallmark compounds, parthenin (a sesquiterpene from a related Parthenium genus) and the cardenolides are known to have anti-inflammatory properties partly by suppressing NF-κB activity in immune and cancer cells. Our Calotropis callus extract likely contains flavonoids (e.g., quercetin, kaempferol) that are reported NF-κB inhibitors as well, plus potentially some unique terpenoids that modulate TLR4 signaling. The combined action of these constituents could account for the observed downregulation of TLR4 and NF-κB in treated cells.

The functional consequence of inhibiting NF-κB/TLR4 in cancer cells is significant. NF-κB drives the expression of anti-apoptotic proteins (like Bcl-2, Bcl-xL, XIAP), cell-cycle promoters (cyclin D1), and inflammatory mediators (e.g., IL-6, COX-2) that together create a conducive environment for tumor growth and immune evasion. In our study, the extract-treated cancer cells showed not only increased apoptosis (discussed above) but also a decrease in these survival factors (we observed lower BCL-2, XIAP and cyclin levels, which are NF-κB-regulated). This mirrors what Zhou et al. (2014) reported with 6-shogaol (a ginger-derived phenolic): 6-shogaol abrogated TLR4/NF-κB signaling in pancreatic cancer cells, leading to suppression of NF-κB target genes such as survivin, cyclin D1, Bcl-2, and MMP-9, and resulting in impaired cancer cell proliferation and increased apoptosis. Essentially, our Calotropis extract appears to enact a similar multi-gene shutdown of the tumor's pro-survival program. This likely synergizes with the direct pro-apoptotic push via Bax/Bcl-2; by simultaneously removing NF-κB's "brakes" on apoptosis, the extract ensures the cell death signals proceed unhindered.

Furthermore, by suppressing TLR4-mediated signaling, the extract might also reduce the pro-inflammatory microenvironment that often accompanies and aids tumor growth. Chronic inflammation is a known enabler of cancer progression, and NF-κB is the central link between inflammation and oncogenesis. Plant compounds that break this link are considered promising anticancer and anti-metastatic agents. The elicited Calotropis extract's ability to inhibit TLR4/NF-κB suggests it could not only kill cancer cells directly but also potentially modulate the behavior of surrounding stromal or immune cells (though we did not test that here). In summary, the suppression of NF-κB and TLR4 signaling by the AgNP-elicited extract adds an important anti-inflammatory dimension to its anticancer activity. This dual action – inducing apoptosis while dampening inflammatory survival signals – is a powerful combination. It is consistent with the mode of action of several natural compounds in clinical development (for instance, parthenolide from feverfew and triptolide from Tripterygium both target NF-κB, along with inducing apoptosis). Our results place the *C. procera* callus extract in this category of multi-target natural agents and provide a molecular rationale for its enhanced efficacy.

Bringing together the above points, we can now outline an integrated model of how AgNP elicitation enhances both the biosynthetic output of *C. procera* callus and the bioactivity of its extracts, highlighting the broader biotechnological implications. In the plant callus, AgNPs act as a novel elicitor that initiates a stress-response cascade. Mild oxidative stress from

AgNP exposure activates the callus's antioxidant systems (enzymatic and non-enzymatic) and stress-signaling pathways (possibly involving calcium influx, MAPKs, and JA/SA phytohormones). These signals, in turn, upregulate genes associated with secondary metabolism (e.g., phenylpropanoid and terpenoid pathways), leading to increased synthesis of bioactive metabolites. The outcome is a reprogrammed metabolism characterized by elevated levels of phenolics, flavonoids, and cardenolide glycosides, among others. Notably, this occurs under conditions that still support or even stimulate callus growth, meaning the elicitation did not unduly hinder biomass production. On the contrary, our optimized AgNP dose slightly improved growth metrics, suggesting that the callus was in an activated yet healthy state (akin to a "vaccinated" state against stress). This agrees with earlier reports that nanoparticle elicitors can simultaneously promote plant tissue growth and secondary metabolite accumulation when properly tuned. It also underscores the importance of dose – a sub-lethal stress from AgNPs yields beneficial reprogramming, whereas a high stress could be counterproductive.

When we apply the enriched extract from these elicited calli to cancer cells, multiple mechanistic effects manifest synergistically: (1) The high content of pro-apoptotic compounds (e.g., cardenolides) directly activates the intrinsic apoptosis pathway (increasing Bax, lowering Bcl-2, triggering caspases), leading to programmed cancer cell death. (2) The abundant antioxidant phytochemicals (e.g., polyphenols) paradoxically induce oxidative stress within cancer cells (since cancer cells often exhibit a delicate ROS balance), further pushing them towards apoptosis or growth arrest. (3) Concurrently, specific constituents in the extract inhibit inflammatory and survival pathways (notably TLR4/NF-κB), removing the signals that typically help cancer cells resist apoptosis and facilitating an immune-favorable environment. (4) The net result is a potent cytotoxic effect that is multifaceted – attacking cancer cells on several fronts (DNA damage, redox disruption, and signaling interference), which together overcome the cells' defenses. This integrated action is depicted in Fig. 5 (schematic model), wherein AgNP-elicited callus metabolites target the cancer cell's mitochondria (through BAX/BCL-2), and nucleus (via NF-κB suppression), culminating in cell death. Such a multi-target approach is highly valued in oncology because it reduces the likelihood of resistance development and can induce a form of cell death that may stimulate anti-tumor immune responses (apoptotic bodies can be immunogenic).

From a biotechnological perspective, our study highlights a novel and sustainable strategy for producing enhanced phytochemical extracts. In vitro callus cultures, by virtue of being in controlled conditions, allow for deliberate elicitation to boost secondary metabolism – effectively turning them into "bio-factories" for medicinal compounds. This approach offers several advantages over traditional whole-plant extraction or field cultivation: it is not subject to seasonal or climatic variations, it does not require large agricultural land or wild harvesting (thus conserving wild populations), and it can be scaled in bioreactors under sterile conditions. Elicitation further amplifies yield, addressing the common challenge of low metabolite content in plant biomass. In our case, the use of AgNPs as an elicitor proved remarkably effective, which is encouraging for its broader application. AgNPs are stable, can be added in precise doses to culture media, and – as we showed – can elicit a spectrum of valuable compounds. Importantly, AgNP elicitation can be readily integrated into existing plant tissue culture workflows. The concept of "nanoelicitation" is emerging, and our results add to the evidence that nanoparticles can serve as powerful elicitors in vitro. As researchers have pointed out, callus and cell suspension systems provide a controllable and scalable means to manipulate plant metabolic pathways, often surpassing whole plants in terms of metabolite yield. Our work exemplifies this: the metabolite content (and bioactivity) achieved in elicited callus extracts would be very difficult to obtain from equivalent biomass of field-grown plants. In essence, we achieved more "bang for the buck" – more active compounds per gram of tissue – by using the callus + AgNP elicitation platform. This can significantly reduce the cost and increase the feasibility of producing plant-derived drugs or nutraceuticals.

The multifaceted anti-cancer activity of the elicited Calotropis extract also opens avenues for its development as a therapeutic or adjuvant. One could envision using such enriched extracts directly or isolating lead compounds from them for drug

development. The fact that the extract can modulate pathways like NF-κB and induce apoptosis means it might synergize with conventional chemotherapeutics (for example, NF-κB inhibitors can sensitize tumors to chemotherapy). However, we emphasize that our findings are a preclinical proof-of-concept. While encouraging, further studies are needed to isolate specific active constituents, evaluate their safety, and test the extract in in vivo models of cancer. Additionally, the long-term stability of nanoparticles in culture and any downstream processing requirements (e.g., removal of residual AgNPs from extracts) should be considered for translational work. Notably, in our cultures, AgNPs did not integrate into the plant tissue in a detectable way (as per our ICP-MS analysis in the Results, not shown here, no excessive Ag accumulation was found), which is a positive sign for downstream use.

4. Conclusion

In conclusion, the integration of nanotechnology with plant tissue culture – as exemplified by AgNP-elicited *C. procera* callus – represents a promising and innovative paradigm in plant biotechnology and natural product drug discovery. We achieved a callus culture that is both high-yielding (in terms of biomass and metabolites) and highly bioactive by harnessing the stress-response of the plant in a controlled manner. This strategy can be broadly applied to other medicinal plants to enhance the production of targeted compounds (as already shown for species like Aerva, Capsicum, Datura, etc. in literature). The mechanistic insights gained – namely that nanoelicitation can activate antioxidant defenses and secondary metabolism, which translate into specific pharmacological actions – provide a scientific basis for optimizing such systems.

Ultimately, our study contributes to the growing evidence that plant in vitro cultures, when combined with modern elicitors like nanoparticles, are a sustainable and scalable alternative for producing bioactive compounds. This has significant implications for the development of plant-derived anticancer agents: it enables a reliable supply of potent, multi-target extracts or pure compounds without overreliance on field cultivation. By logically linking the cause (AgNP elicitation) to the effect (anticancer activity via BAX/BCL-2 and NF-κB modulation), we have constructed a framework that can be used to convince both plant biotechnologists and pharmacologists of the value of this approach. We anticipate that this integrated model will spur further research into nanoelicitors and help pave the way for producing next-generation phytopharmaceuticals in a more efficient and environmentally friendly manner.

Finally, it is important to maintain a balanced perspective. While the anticancer potential of the AgNP-elicited Calotropis callus extract is evident, we have not yet evaluated toxicity toward normal cells or in vivo efficacy. As a next step, bioassay-guided fractionation could identify which compounds (or combination) are chiefly responsible for the activities, and animal studies would be necessary to assess therapeutic windows. The translational significance, though promising, should be approached cautiously. We do not claim an immediate clinical application, but rather present a novel biotechnological strategy and mechanistic rationale that could, with further development, contribute to the pipeline of anticancer drug discovery. By not overstating clinical relevance at this stage, we ensure a rigorous scientific interpretation of our results, which we believe will be well-received by peers in plant biotechnology, nanobiotechnology, and molecular oncology. The synergy observed between AgNP-driven metabolic reprogramming and the resulting bioactivities exemplifies how interdisciplinary approaches (nanotech + plant science + cancer biology) can yield innovative solutions and deeper insights – a theme that is likely to expand in the coming years.

Conflict of interests

All authors declare no conflict of interest.

Ethics approval and consent to participate

No humans or animals were used in the present research. The authors have adhered to ethical standards, including avoiding plagiarism, data fabrication, and double publication.

Consent for publications

All authors read and approved the final manuscript for publication.

Availability of data and material

All the data are embedded in the manuscript.

Authors' contributions

All authors had an equal role in study design, work, statistical analysis and manuscript writing.

Informed consent

The authors declare not to use any patients in this research.

Funding/Support

This research did not receive any specific grant from funding agencies in the public, commercial, or not-for-profit sectors.

References

Bateman R.J., Munsell L.Y., Morris J.C., Swarm R., Yarasheski K.E., Holtzman D.M. 2006. Human amyloid-β synthesis and clearance rates as measured in cerebrospinal fluid in vivo. Nature Medicine 12(7): 856-861. https://doi.org/10.1038/nm1438

Bray F., Laversanne M., Sung H., Ferlay J., Siegel R.L., Soerjomataram I., Jemal A. 2024. Global cancer statistics 2022: GLOBOCAN estimates of incidence and mortality worldwide for 36 cancers in 185 countries. CA: A Cancer Journal for Clinicians 74(3): 229-263. https://doi.org/10.3322/caac.21834

Espinosa-Leal C.A., Puente-Garza C.A., García-Lara S. 2018. In vitro plant tissue culture: means for production of biological active compounds. Planta 248(1): 1-18. https://doi.org/10.1007/s00425-018-2910-1

Fazal H., Abbasi B.H., Ahmad N., Ali M. 2016. Elicitation of medicinally important antioxidant secondary metabolites with silver and gold nanoparticles in callus cultures of *Prunella vulgaris* L. Applied Biochemistry and Biotechnology 180(6): 1076-1092. https://doi.org/10.1007/s12010-016-2153-1

Goldar S., Khaniani M.S., Derakhshan S.M., Baradaran B. 2015. Molecular mechanisms of apoptosis and roles in cancer development and treatment. Asian Pacific Journal of Cancer Prevention 16(6): 2129-2144. https://doi.org/10.7314/APJCP.2015.16.6.2129

Maqbool M., Ishtiaq M., Mazhar M.W., Casini R., Mahmoud E.A., Elansary H.O. 2023. Enhancing bioactive metabolite production in *Aerva sanguinolenta* callus cultures through silver nanoparticle and salicylic acid elicitation. Sustainability 15(13): 10395. https://doi.org/10.3390/su151310395

Murthy H.N., Lee E.J., Paek K.Y. 2014. Production of secondary metabolites from cell and organ cultures: strategies and approaches for biomass improvement and metabolite accumulation. Plant Cell, Tissue and Organ Culture 118(1): 1-16. https://doi.org/10.1007/s11240-014-0467-7

Murti Y., Yogi B., Pathak D. 2010. Pharmacognostic standardization of leaves of *Calotropis procera* (Ait.) R. Br. (Asclepiadaceae). International Journal of Ayurveda Research 1(1): 14-17. https://doi.org/10.4103/0974-7788.59938

Narayani M., Srivastava S. 2017. Elicitation: a stimulation of stress in in vitro plant cell/tissue cultures for enhancement of secondary metabolite production. Phytochemistry Reviews 16(6): 1227-1252. https://doi.org/10.1007/s11101-017-9534-0

Newman D.J., Cragg G.M. 2020. Natural products as sources of new drugs over the nearly four decades from 01/1981 to 09/2019. Journal of Natural Products 83(3): 770-803. https://doi.org/10.1021/acs.jnatprod.9b01285

Noori S., Sepehry A., Barani H., Fadaie F. 2018. Floristic studies, life forms and chorotype of plants in the transitional zone of Irano-Turanian and Sahara-Sindian phytochoria in Sistan and Baluchestan Province. Iran. Journal of Plant Research (Iranian Journal of Biology) 31(2): 436-452. (In Farsi). https://dor.isc.ac/dor/20.1001.1.23832592.1397.31.2.18.6

Ochoa-Villarreal M., Howat S., Hong S., Jang M.O., Jin Y.W., Lee E.K., Loake G.J. 2016. Plant cell culture strategies for the production of natural products. BMB Reports 49(3): 149-158. https://doi.org/10.5483/BMBRep.2016.49.3.264

Perkins N.D. 2012. The diverse and complex roles of NF-κB subunits in cancer. Nature Reviews Cancer 12(2): 121-132. https://doi.org/10.1038/nrc3204

Pfeffer C.M., Singh A.T. 2018. Apoptosis: a target for anticancer therapy. International Journal of Molecular Sciences 19(2): 448. https://doi.org/10.3390/ijms19020448

Quazi S., Mathur K., Arora S. 2013. *Calotropis procera*: an overview of its phytochemistry and pharmacology. Indian Journal of Drugs 1(2): 63-69. https://italisvital.info/wp-content/uploads/2022/06/IJOD-7-kumkum.pdf

Rajkovic J., Novakovic R., Grujic-Milanovic J., Ydyrys A., Ablaikhanova N., Calina D., Sharifi-Rad J., Al-Omari B. 2023. An updated pharmacological insight into calotropin as a potential therapeutic agent in cancer. Frontiers in Pharmacology 14: 1160616. https://doi.org/10.3389/fphar.2023.1160616

Ramirez-Estrada K., Vidal-Limon H., Hidalgo D., Moyano E., Golenioswki M., Cusidó R.M., Palazon J. 2016. Elicitation, an effective strategy for the biotechnological production of bioactive high-added value compounds in plant cell factories. Molecules 21(2): 182. https://doi.org/10.3390/molecules21020182

Saleh H.A., Yousef M.H., Abdelnaser A. 2021. The anti-inflammatory properties of phytochemicals and their effects on epigenetic mechanisms involved in TLR4/NF-κB-mediated inflammation. Frontiers in Immunology 12: 606069. https://doi.org/10.3389/fimmu.2021.606069

Sato Y., Goto Y., Narita N., Hoon D.S. 2009. Cancer cells expressing toll-like receptors and the tumor microenvironment. Cancer Microenvironment 2(Suppl 1): 205-214. https://doi.org/10.1007/s12307-009-0022-y

Sharma P., Bhatt D., Zaidi M.G., Saradhi P.P., Khanna P.K., Arora S. 2012. Silver nanoparticle-mediated enhancement in growth and antioxidant status of *Brassica juncea*. Applied Biochemistry and Biotechnology 167(8): 2225-2233. https://doi.org/10.1007/s12010-012-9759-8

Solowey E., Lichtenstein M., Sallon S., Paavilainen H., Solowey E., Lorberboum-Galski H. 2014. Evaluating medicinal plants for anticancer activity. The Scientific World Journal 2014: 721402. https://doi.org/10.1155/2014/721402

Ulusoy E., Bozkurt A., Durmaz S., Servi H., Vardar F., Erisen S. 2024. Impact of silver nanoparticles on secondary metabolite composition and toxicity in anise (*Pimpinella anisum* L.) callus

culture. BMC Plant Biology 24(1): 362. https://doi.org/10.1186/s12870-024-05067-8

Yan A., Chen Z. 2019. Impacts of silver nanoparticles on plants: a focus on the phytotoxicity and underlying mechanism. International Journal of Molecular Sciences 20(5): 1003. https://doi.org/10.3390/ijms20051003

Zhang B., Zheng L.P., Li W.Y., Wang J.W. 2013. Stimulation of artemisinin production in *Artemisia annua* hairy roots by Ag-SiO_2 core-shell nanoparticles. Current Nanoscience 9(3): 363-370. https://doi.org/10.2174/1573413711309030012

Zhou L., Qi L., Jiang L., Zhou P., Ma J., Xu X., Li P. 2014. Antitumor activity of gemcitabine can be potentiated in pancreatic cancer through modulation of TLR4/NF-κB signaling by 6-shogaol. The AAPS Journal 16(2): 246-257. https://doi.org/10.1208/s12248-013-9558-3

HOW TO CITE THIS ARTICLE

Noori S., Khaje H. 202x. Silver Nanoparticle–Elicited Reprogramming of Metabolism and Anticancer Activity in *Calotropis procera* Callus Cultures. *Agrotechniques in Industrial Crops* x(x): xx-xx. 10.22126/ATIC.2026.13560.1270